

Exploiting Latent Linearity in LLMs Improves Explainable Molecular Representation Learning

Zhuoran Li, Xu Sun, Wanyu Lin*, *Member, IEEE*, Jiannong Cao, *Fellow, IEEE*

Abstract—Large language models (LLMs) have demonstrated broad utility across molecular domains, spanning drug discovery and materials design. Analyzing LLMs’ latent representations is crucial for elucidating their underlying mechanisms, improving explainability, and ultimately advancing downstream performance. We propose *MoleX*, a simple yet effective framework that decomposes molecular embeddings within LLM representations into a concept-aligned space for explainable molecular representation learning. We further show that these high-dimensional embeddings admit a linear mapping onto chemically consistent concepts. Our analysis suggests that the uncovered linearity aligns with established chemical principles, indicating a mechanistically explainable latent structure in LLM representations for scientific applications. When applied to downstream tasks, this latent linearity improves both predictive and explanatory performance. Extensive experiments demonstrate that *MoleX* outperforms existing approaches in accuracy, explainability, and efficiency—achieving CPU inference on large-scale datasets 300× faster with 100,000 fewer parameters than LLMs.

Index Terms—Molecular representation learning, explainability, molecular property prediction, large language models.

I. INTRODUCTION

MOLECULAR property prediction exemplifies a fundamental scientific task that infers molecular properties from given structures, serving as a cornerstone in fields such as computational chemistry and biology [1]–[7]. Modern LLMs have achieved exceptional predictive performance by learning expressive molecular representations that capture chemical semantics from large textual corpora [8]–[14]. However, LLMs remain mechanistically opaque due to their black-box nature [15]–[17]: *why do these representations work, and can we trust what they learn?* Though prior efforts identify key substructures linked to properties, few derive them from the model’s representational mechanisms, reducing explanation faithfulness. Among them, description-based approaches [18] are hindered by descriptive subjectivity and the complexity of molecular patterns [19], [20], while attention-based methods [21], [22] often fail to reflect true feature importance [23].

Zhuoran Li is with the Department of Computing, The Hong Kong Polytechnic University, Hong Kong SAR, P.R. China (e-mail: zhuor5.li@connect.polyu.hk).

Xu Sun is with the Department of Computing, The Hong Kong Polytechnic University, Hong Kong SAR, P.R. China (e-mail: yeluo.sun@connect.polyu.hk).

Wanyu Lin is with the Department of Computing and Department of Data Science and Artificial Intelligence, The Hong Kong Polytechnic University, Hong Kong SAR, P.R. China (e-mail: wan-yu.lin@polyu.edu.hk).

Jiannong Cao is with the Department of Computing, The Hong Kong Polytechnic University, Hong Kong SAR, P.R. China (e-mail: jian-nong.cao@polyu.edu.hk).

(*Corresponding author: Wanyu Lin.)

Notably, *Lamole* [24] provides a state-of-the-art solution that delivers both accurate and explainable predictions, but it remains highly model-specific [25] and offers only local explanations [26]. In summary, these studies do not adequately illuminate how molecular structures are encoded in latent space and how those encodings produce the predicted properties.

To address the limitations, we exploit LLMs’ hidden representations to develop a mechanistically explainable approach that is robust to input sensitivity, model specificity, and interpretive subjectivity. Conceptually, LLM representations encode the model’s latent reasoning patterns for a given input (*i.e.*, how the LLM uses its “knowledge” to reason) [27]–[29], so understanding them is key to unlocking LLMs’ full potential in scientific tasks [30]. To achieve domain-aligned explainability, we aim to map these representations to chemically meaningful concepts. Inspired by the linear representation hypothesis [31], [32], we investigate whether and how LLM-derived molecular representations can be *linearly decomposed* into chemical concepts (as shown Figure 2). Although LLMs are built on complex nonlinear transformations, we posit that operative molecular semantics reside in an approximately linear geometry with respect to *functional groups*, which are widely adopted concepts for property attribution in molecular science [33]–[37]. In particular, we achieve this by feeding Group SELFIES [38], a textual representation that partitions molecules into functional group units (see Supplementary Material I for an visualized illustration), into the LLM to obtain functional-group-based tokens for our subsequent study.

In light of this, we introduce *MoleX* (outlined in Figure 1), which constructs a low-dimensional conceptual space spanned by functional group vectors and learns a sparse linear mapping from LLM-derived representations onto this space. Each molecule is represented as a weighted combination of concepts, with weights reflecting predictive significance. This yields concept-level explanations grounded in chemical principle while maintaining strong predictive performance. However, while LLMs encode rich molecular semantics, simple linear representations may fail to capture intricate patterns, leading to mispredictions on complex tasks. To address this, we design a residual calibration strategy that iteratively corrects prediction errors from the base linear predictor. Beyond improving predictive accuracy, residual calibration also increases explanation faithfulness by progressively probing molecular substructures that are chemically consistent with the ground truth. We summarize our main contributions as follows:

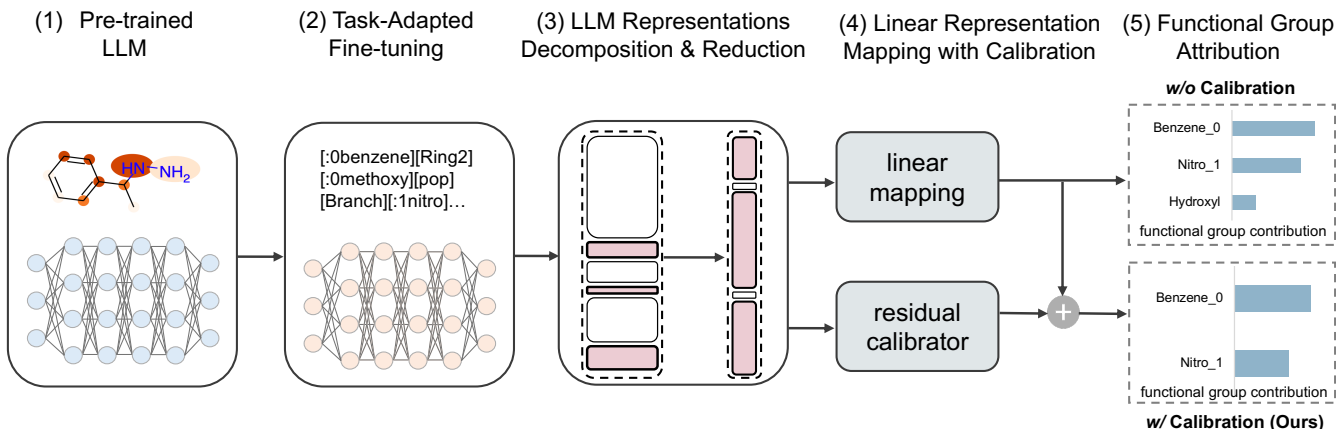


Fig. 1: **The overview of *MoleX***: (1) employ ChemBERTa-2 as the foundation model, (2) fine-tune it using a tailored objective to retain maximal task-relevant semantics, (3) decompose and project latent representations onto chemically meaningful concepts, (4) train a linear predictor on the derived concepts, (5) incorporate residual calibration to iteratively refine model predictions.

- 1) We propose a chemically consistent decomposition framework that reveals hidden linearity in LLMs’ latent geometry, enhancing mechanistic explainability in molecular representation learning.
- 2) We design a residual calibration strategy to compensate for the linear predictor’s limited expressiveness, improving both predictive accuracy and explanation faithfulness.
- 3) We demonstrate that *MoleX* achieves state-of-the-art accuracy, explainability, and efficiency on benchmark molecular property prediction tasks with over 100,000 fewer parameters than existing deep models.
- 4) We present a theoretical analysis of how latent linearity boosts explainability, providing provable insights for molecular property prediction.

Empirical evidence confirms that linear structure exists in LLMs’ representational geometry and can be expressed as a combination of chemical concepts. Relying solely on simple techniques, *MoleX* provides meaningful insight into understanding complex LLM representations from the view of domain knowledge. Moreover, we introduce a residual calibration approach to capture errors from the base linear predictor, further improving both accuracy and explainability. Taken together, *MoleX* demonstrates that latent linearity in LLMs provides a principled basis for effective and explainable molecular representation learning. When used for molecular property prediction, the exploited linearity notably improves predictive accuracy, explanation faithfulness, and computational efficiency, underscoring its applicability in practical scenarios.

II. RELATED WORK

Explainable Molecular Representation Learning. Molecules can naturally be modeled as graphs, so that many explainable GNNs have been proposed to capture structure–property relationships [39], [40]. However, their explanations typically focus on atom- or bond-level importance, which often lack chemical consistency and fail to reflect higher-level functional group interactions. In contrast, LLMs

have shown strong capabilities in learning substructure-level interactions from text-based molecular representations [8], [24], [41]. Despite their expressive power, LLMs remain opaque, raising concerns about faithfulness and reliability, especially in safety-critical domains such as drug design [42]. Our approach bridges this gap by aligning LLM-based chemical concepts with a transparent linear predictor, enabling both accurate predictions and chemically consistent explanations.

Explainability Methods for LLMs. To interpret LLMs, various explanation techniques have been proposed. Gradient-based methods estimate input importance via output derivatives [43], but their sensitivity to perturbations limits robustness [44], [45]. Attention-based methods rely on attention weights [46], yet these weights can not faithfully reflect model reasoning [25], [47]. Perturbation-based methods analyze output changes under input modifications [48], but often suffer from instability due to randomness in the perturbation process [49]. In contrast, our method directly decomposes LLM representations into interpretable chemical concepts and applies an explainable linear mapping for prediction, combining the expressive power of LLMs with the simplicity and faithfulness of linear predictor to produce accurate and explainable outputs.

III. PRELIMINARIES

Let $\mathcal{G} = \{(g^{(i)}, y^{(i)})\}$ be a dataset of molecular graphs $g^{(i)}$ and their properties $y^{(i)}$. Our goal is to predict y from molecular structure while providing explanations that remain aligned with chemically meaningful substructures, namely functional groups. We first convert each $g^{(i)}$ into Group SELFIES, denoted as $x^{(i)} = \{x_1^{(i)}, \dots, x_{j^{(i)}}^{(i)}\}$, where $x_j^{(i)}$ is the j -th group. We fine-tune an LLM f for molecular property prediction and obtain its representation $f(x)$ (i.e., the latent representation of x). The overall predictor consists of an explainable linear predictor h and a residual calibrator r . Concretely, we first compress $f(x)$ into a low-dimensional principal component analysis (PCA) representation $z(x)$, and split the PCA dimensions into two disjoint index sets I_H and

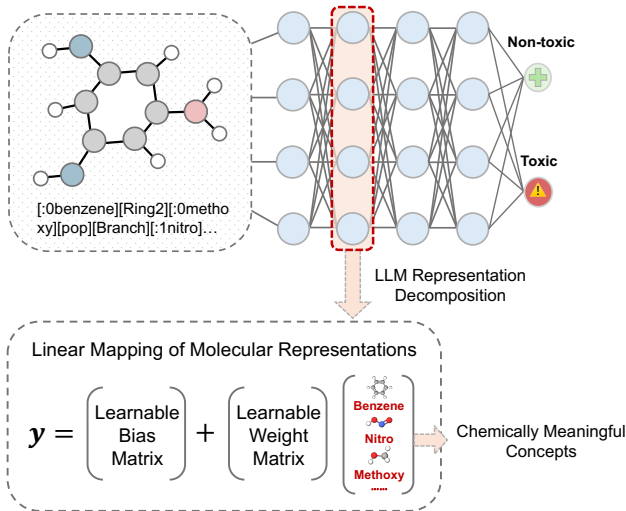


Fig. 2: The molecular representations are decomposed into a linear mapping of functional groups.

I_R with $I_H \cap I_R = \emptyset$. We denote the corresponding subvectors by $f_H(x)$ and $f_R(x)$ (in our implementation, $f_H(x) = z_H(x)$ and $f_R(x) = z_R(x)$). This construction yields non-overlapping features for the linear predictor and the residual calibrator, so their effects are separable in the logit space.

Specifically, we first train h on $f_H(x)$ and then freeze its parameters. Next, we train r on $f_R(x)$ to correct the prediction errors of the base predictor h by minimizing:

$$\min_r \mathbb{E}_{(x,y) \sim \mathcal{D}} [\mathcal{L}(\sigma(h(f_H(x)) + r(f_R(x))), y)], \quad (1)$$

where \mathcal{D} is the training dataset, and $h(\cdot)$ and $r(\cdot)$ can be interpreted as logits. Building on [50], we use coefficients in the linear predictor to quantify feature effect on property y . Let $[f_H(x)]_j$ be the j -th explainable feature and let w_j be its coefficient in h . Then the instance-level contribution score is computed as $c_j = w_j [f_H(x)]_j$, which measures the contribution of that feature to the prediction under the linear predictor. Therefore, we can statistically quantify the contribution of the j -th functional group to property y . For simplicity, we omit the superscript (i) in the following descriptions.

IV. OUR FRAMEWORK: *MoleX*

The proposed approach leverages simple yet principled tools from statistical machine learning to exploit latent linearity within the intricate representational geometry of LLMs. Specifically, *MoleX* consists of two stages: (1) decomposing high-dimensional molecular representations into chemical concepts, and (2) learning a concept-level linear mapping with residual calibration. Our design is motivated by a simple goal: preserve the expressive power of LLM representations, but uncover the task-relevant information through a small set of explainable features that can be statistically attributed.

In particular, we first fine-tune a pre-trained LLM using an information bottleneck-inspired objective to construct informative molecular representations. The resulting embeddings are then decomposed at the functional-group level, and we further apply dimensionality reduction to obtain a compact latent space suitable for linear modeling. A linear predictor h is trained on

an explainable subset of these features to predict molecular properties, while a residual calibrator r corrects the remaining errors in logit space using the complementary feature subset. The final prediction subsequently combines both h and r to yield accurate and explainable results.

A. Constructing and Decomposing LLM Representations

LLM Fine-Tuning. To learn informative representations, we fine-tune the LLM on Group SELFIES, aligning input tokens with chemically consistent substructures. In our task, this step encourages the latent representation to emphasize chemically meaningful patterns (e.g., functional-group-level semantics) rather than spurious molecular fragments. Nevertheless, standard fine-tuning often entangles molecular semantics with irrelevant noise. To address this, we introduce a fine-tuning objective inspired by the variational information bottleneck (VIB) [51]. Intuitively, we want the latent representation e to maximally retain information predictive of the property y while discarding redundant details from the molecular structure x that do not support explainable structure–property reasoning.

Given a molecular input x , property y , and the LLM’s latent representation e , we define $p_0(e)$ as the prior over e , and $q_\theta(y | e)$ as a variational approximation to the conditional distribution of y given e . We quantify the desired trade-off using mutual information: $I(e; y)$ measures how predictive the representation is for the downstream property, while $I(e; x)$ measures how much input information is preserved. The mutual information between e and y is given by:

$$I(e; y) = \mathbb{E}_{p(e,y)} \left[\log \frac{p(e,y)}{p(e)p(y)} \right] = \mathbb{E}_{p(e,y)} \left[\log \frac{p(y|e)}{p(y)} \right],$$

and we introduce the variational decoder $q_\theta(y | e)$ and optimize the tractable surrogate $\mathbb{E}_{p_\theta(e|x)} [-\log q_\theta(y | e)]$. The mutual information between e and x is defined as:

$$\begin{aligned} I(e; x) &= \mathbb{E}_{p(e,x)} \left[\log \frac{p(e | x)}{p(e)} \right] \\ &= \mathbb{E}_{p(x)} [D_{\text{KL}}(p_\theta(e | x) \| p(e))]. \end{aligned}$$

Since the marginal distribution $p_\theta(e)$ is intractable, we approximate it with the prior $p_0(e)$. Under this approximation,

$$\mathbb{E}_{p(x)} [D_{\text{KL}}(p_\theta(e | x) \| p_0(e))] = I(e; x) + D_{\text{KL}}(p_\theta(e) \| p_0(e))$$

provides a tractable upper bound on $I(e; x)$ up to an x -independent term, which allows us to control (i.e., an upper-bound) the mutual information between e and x . Inspired by [52], we approximate encoder $p_\theta(e | x)$ by a Gaussian distribution. Let $f_e^\mu(x)$ and $f_e^\Sigma(x)$ be neural networks that output the mean and covariance matrix of latent variable e , then the encoder can be expressed as $p_\theta(e | x) = \mathcal{N}(e | f_e^\mu(x), f_e^\Sigma(x))$. Applying the reparameterization trick, we sample e as $e = f_e^\mu(x) + f_e^\Sigma(x)^{1/2} \cdot \epsilon$, where $\epsilon \sim \mathcal{N}(0, I)$. Eventually, we design the LLM fine-tuning objective as:

$$\begin{aligned} \mathcal{L}(\theta) &= \sum_{(x,y) \in \mathcal{S}_F} \left(\mathbb{E}_{p_\theta(e|x)} [-\log q_\theta(y | e)] + \right. \\ &\quad \left. \beta \cdot D_{\text{KL}}(p_\theta(e | x) \| p_0(e)) \right), \end{aligned} \quad (2)$$

where β controls the trade-off between compression and performance, q_θ serves as the decoder, and \mathcal{S}_F denotes the fine-tuning dataset. Specifically, the first term, $\mathbb{E}_{p_\theta(e|x)}[-\log q_\theta(y|e)]$, encourages the latent representation e to retain task-relevant information about y . The second term, $\beta \cdot D_{\text{KL}}(p_\theta(e|x) \| p_0(e))$, regularizes e toward the prior to limit information captured from x that is not necessary for predicting y . In summary, this objective ensures that the fine-tuned LLM learns representations e that retain maximal task-relevant semantics from y while suppressing redundancy from x . By constraining information flow, our method highlights chemically contributory information while filtering irrelevant content, thereby enhancing specificity and explainability for molecular representation learning. We formulate this guarantee as follows (demonstration provided in the Supplementary Material A).

Remark IV.1. Let $\mathcal{L}(\theta)$ denote the loss in Equation (2). Minimizing $\mathcal{L}(\theta)$ encourages the learned molecular representations e to balance predictive accuracy via the negative log-likelihood term and compression toward the prior via the KL regularization, which serves as an information-bottleneck-inspired inductive bias for molecular property prediction.

Representation Decomposition. We begin by encoding each molecule using Group SELFIES, a structured molecular representation that preserves functional group boundaries by design. We train a functional group-level tokenizer that individually processes each token/functional group, which is then passed through the fine-tuned LLM to obtain a fixed-size embedding. This design reduces interference between tokens and enables clear attribution of learned features to their corresponding functional groups. Finally, to obtain a global representation, we aggregate the local embeddings of all functional groups within a molecule into a single vector. This vector retains the semantic expressiveness of LLM representations while preserving a decomposition aligned with chemical concepts. In essence, we decompose high-dimensional molecular representations into functional group vectors and aim to explain each group’s contribution to the predicted property. We use UMAP [53] to visualize the decomposed functional group semantics in 3D space, as shown in Figure 3 (more visualizations are provided in the Supplementary Material F).

B. Learning a Linear Mapping with Residual Calibration

Dimensionality Reduction. LLM-derived molecular embeddings are high-dimensional and contain redundant chemical semantics that can obscure information relevant to molecular property prediction. Therefore, dimensionality reduction is needed before learning a predictor. In this work, we leverage PCA as it provides a statistically explainable way to compress representations [54]. Specifically, PCA projects high-dimensional LLM embeddings onto orthogonal directions of maximal explained variance, producing compact representations in which we can later separate explainable and residual components for calibration.

Formally, let $f(x) \in \mathbb{R}^d$ denote the LLM representations of molecule x , and let \mathcal{S}_D be the dataset used to run the PCA.

We define the empirical mean as $\mu := |\mathcal{S}_D|^{-1} \sum_{(x,y) \in \mathcal{S}_D} f(x)$, and the empirical covariance as:

$$\Sigma := |\mathcal{S}_D|^{-1} \sum_{(x,y) \in \mathcal{S}_D} (f(x) - \mu)(f(x) - \mu)^\top \in \mathbb{R}^{d \times d}.$$

PCA aims to learn an orthonormal loading matrix $U_k \in \mathbb{R}^{d \times k}$ such that $U_k^\top U_k = I_k$ to maximize the retained variance:

$$U_k = \arg \max_{U \in \mathbb{R}^{d \times k} : U^\top U = I_k} \text{Tr}(U^\top \Sigma U),$$

whose solution consists of the top- k eigenvectors of Σ with eigenvalues $\lambda_1 \geq \dots \geq \lambda_d$. The original molecular representation is then reduced by projection as follows:

$$z(x) := U_k^\top (f(x) - \mu) \in \mathbb{R}^k,$$

so that $z(x)$ provides a compact representation for downstream tasks. In our setting, these PCA coordinates serve as a denoised latent space where linear predictors can capture dominant structure–property signals. The dimension k is chosen by an explained-variance threshold $\sum_{i=1}^k \lambda_i / \sum_{i=1}^d \lambda_i \geq \tau$ or via validation on the molecular property y (i.e., we include an empirical study in Section V-C to illustrate how to determine the optimal k). The parameters (μ, U_k) are estimated once on \mathcal{S}_D and then fixed for subsequent linear mapping. Accordingly, we extract statistically relevant dimensions from noisy latent space. Noteworthy, after each functional-group token is encoded by the LLM and then dimension-reduced, we construct a mapping table linking each functional group to its corresponding reduced molecular embedding. This allows us to trace each feature back to a specific functional group by looking up this table during attribution with the linear predictor.

Linear Mapping of Concepts. We train a linear predictor on the explainable representation $f_H(\tilde{x}) \in \mathbb{R}^n$ for property prediction. The motivation is that, for molecular tasks, a linear mapping in a concept-aligned space provides a direct link between substructures and predicted properties, which is crucial for chemically grounded explanations. In our implementation, $f_H(\tilde{x})$ corresponds to the explainable PCA subvector $z_H(x)$ (thus $n = |I_H|$). It can be formulated as:

$$h(f_H(\tilde{x})) = \sigma(w^\top f_H(\tilde{x}) + b), \quad w \in \mathbb{R}^n, b \in \mathbb{R},$$

where σ is the sigmoid function. The log-odds then satisfy:

$$\log\left(\frac{h(f_H(\tilde{x}))}{1 - h(f_H(\tilde{x}))}\right) = w^\top f_H(\tilde{x}) + b,$$

so the marginal effect on log-odds with respect to the j -th dimension of $f_H(\tilde{x})$ is

$$\frac{\partial}{\partial [f_H(\tilde{x})]_j} \log\left(\frac{h(f_H(\tilde{x}))}{1 - h(f_H(\tilde{x}))}\right) = w_j.$$

Concretely, this interpretation follows the standard regression theory [55]. The coefficient w_j reflects the per-unit effect on the log-odds along the j -th feature, while the instance-level contribution is $w_j [f_H(\tilde{x})]_j$. Consequently, we can attribute the j -th functional group’s contribution to the molecular property. This suggests an explainable view of how the model’s decision varies along explainable latent dimensions.

Residual Calibration. The linear mapping h , while highly

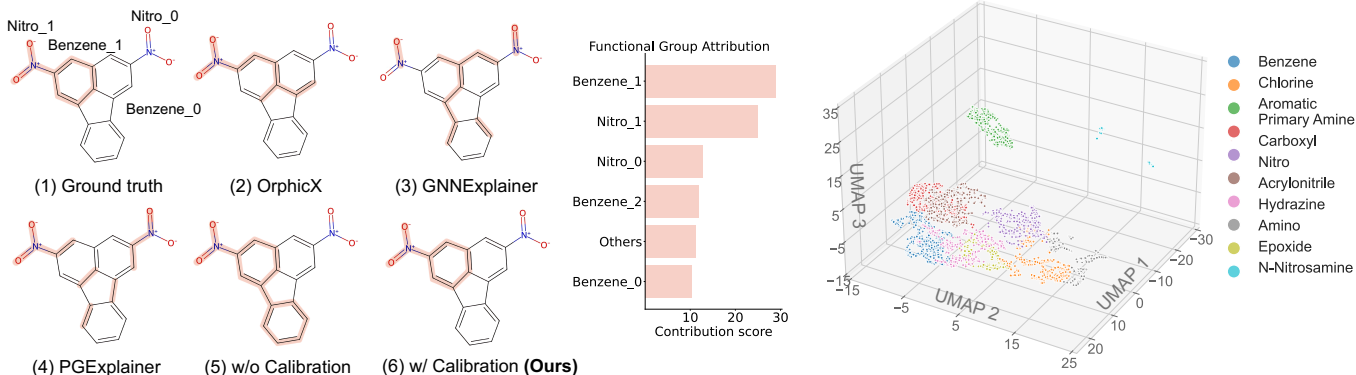


Fig. 3: Illustration of revealed functional groups. **(Left)** Explanation visualization across different methods, with functional group attribution offered by *MoleX*. **(Right)** The 3D UMAP displays well-separated clusters for decomposed functional groups, indicating intrinsic linear structure in the LLM representations with concept-aligned separability. Rare groups form isolated clusters, while chemically related groups remain proximal yet distinguishable, reflecting linearly decodable chemical semantics.

explainable, is inherently limited in expressiveness due to its simple architecture, potentially underfitting complex patterns. We therefore introduce a residual calibrator r that learns an additive correction in logit space while keeping h fixed, so that the overall predictor can improve accuracy without obscuring the attribution of the base linear terms. Concretely, we first compute a PCA representation $z(x) := U_k^\top (f(x) - \mu) \in \mathbb{R}^k$, and then split the PCA coordinates into two disjoint index sets I_H and I_R ($I_H \cap I_R = \emptyset$, $I_H \cup I_R = \{1, \dots, k\}$). We define $z_H(x)$ and $z_R(x)$ as the subvectors of $z(x)$ supported on I_H and I_R , respectively, so that $z(x)$ can be expressed as:

$$z(x) = z_H(x) \oplus z_R(x).$$

This is a coordinate-disjoint split in the PCA coordinate system. We then train the residual calibrator also as a linear function on the residual features as,

$$r(z_R(x)) = w_r^\top z_R(x) + b_r,$$

where $w_r \in \mathbb{R}^{|I_R|}$ and $b_r \in \mathbb{R}$. The base predictor h is a linear logit model on $z_H(x)$, and can be formulated as

$$h(z_H(x)) = \sigma(w_h^\top z_H(x) + b_h).$$

With h frozen, we train r by minimizing the loss in Equation (1), which fits the remaining error not captured by h . The final prediction is then formulated as:

$$\hat{y}(x) = \sigma \left(\underbrace{w_h^\top z_H(x) + b_h}_{\text{base logit}} + \underbrace{w_r^\top z_R(x) + b_r}_{\text{residual logit}} \right).$$

Because z_H and z_R use disjoint PCA dimensions, the contributions from h and r are additively separable at the logit level, and each coefficient in w_h and w_r can be interpreted as the marginal effect of its corresponding feature.

Residual calibration is motivated by a pragmatic mismatch in molecular property prediction: a linear predictor h offers explainable feature attributions but can underfit data, leaving predictive error in the remaining representation. We therefore train r on the complementary feature block and add its output in logit space. This correction refines the decision boundary

without contaminating the main effects made by h . This mechanism typically improves predictive accuracy because r explicitly predicts the residual error not explained by h , while the base predictor is kept fixed to prevent erroneous reallocation of feature contributions. Beyond improving accuracy, residual calibration enhances explainability by recovering missing or mispredicted functional groups, iteratively aligning predictions with chemically consistent substructures. We formalize this guarantee in the following remark (demonstration provided in the Supplementary Material B):

Remark IV.2. Let \mathcal{X} and \mathcal{Y} be the input and output spaces. Let $f : \mathcal{X} \rightarrow \mathbb{R}^d$ be a pre-trained feature mapping, and let $z(x) \in \mathbb{R}^k$ be its PCA representation. Let $h : \mathbb{R}^{|I_H|} \rightarrow \mathcal{Y}$ be a linear mapping operating on the explainable PCA coordinates $z_H(x)$. The residual calibrator $r : \mathbb{R}^{|I_R|} \rightarrow \mathcal{Y}$, defined on the residual PCA coordinates $z_R(x)$, captures the remaining variance not explained by h in an interpretable way, thereby preserving the overall model’s explainability.

Quantifiable Functional Group Contribution. We tokenize Group SELFIES at the functional-group level and encode each group x_j with the LLM individually to obtain semantically meaningful embeddings. We then aggregate these group-wise embeddings and train a linear predictor, where the coefficient w_j associated with x_j quantifies its impact on the target property y . Due to the linearity, $w_j [f_H(\tilde{x})]_j$ measures per-instance contribution score of the j -th functional group to the predicted property, providing a meaningful attribution under the linear modeling assumptions [56]. Furthermore, this enables precise identification of contributory substructures and their interactions from high-dimensional LLM representations. Technically, we map 1D text-based molecules back to their 2D molecular graphs using the contribution scores. By attributing significant functional groups, we identify important nodes and edges in the molecular graph and connect them to highlight contributory substructures. Based on this, we can assess whether the revealed substructure matches the ground truth.

V. EXPERIMENTS

A. Experimental Setup

Datasets. We evaluate *MoleX* on six mutagenicity datasets and one hepatotoxicity dataset. The mutagenicity datasets include Mutag [69], Mutagen [70], and the PTC family [71]; the hepatotoxicity dataset is Liver [72]. To demonstrate *MoleX*'s ability to explain molecular properties using chemically meaningful substructures, we introduce ground truth, substructures verified by domain experts to significantly impact molecular properties. Ground truth annotations for mutagenicity are from [69], [73], and for hepatotoxicity from [38]. To demonstrate the effectiveness of *MoleX*, we further evaluate it on six MoleculeNet datasets: BBBP, Tox21, SIDER, ClinTox, BACE, and HIV [74]. MoleculeNet includes tasks influenced by nonlinear interactions, stereochemistry, and scaffold bias, making it a relatively challenging benchmark. Dataset details are provided in the Supplementary Material C.

Evaluation Metrics. In this study, we evaluate the predictive performance, explainability performance, and computational efficiency of *MoleX*. In particular, we apply a specific metric to assess each of these aspects. For predictive performance, we define $\frac{1}{n} \sum_{i=1}^n \mathbb{I}(y^{(i)} = \hat{y}^{(i)})$ to compute the classification accuracy. For explainability performance, we follow GNNExplainer [75], treating explanations as binary edge classification and using AUC to measure the accuracy. For computational efficiency, we evaluate the execution time for each method.

Moreover, we also assess explanation accuracy against expert-annotated ground truth. As verified by [69], [73], the ground truth substructures for six mutagenicity datasets consist of an aromatic group, such as a benzene ring, bonded with another functional group, such as methoxy, hydroxyl, nitro, or carboxyl groups (note that ground truth exists only for the mutagenic class). For the Liver dataset, the chemist-annotated ground truth includes features such as fused tricyclic saturated hydrocarbon moieties, hydrazines, arylacetic acids, and sulfonamide moieties [72]. We compare whether the substructures revealed by *MoleX* match the ground truth.

Baselines. To extensively compare *MoleX* with advanced methods, we utilize various baselines: (1) GNN baselines (all designed specifically for molecular property prediction), including MolCLR [57], CGIB [58], MoSE [59], FragNet [60], MomentGNN [61], S-CGIB [62], and GraphMVP [63]; (2) LLM baselines, including Llama 3.1-8b [64], GPT-4o [65], and ChemBERTa-2 [9]; (3) explainable machine learning baselines, including logistic regression, decision tree [66], XGBoost [68], and random forest [67].

Implementations. Our model continues pre-training on the full ZINC dataset [76] using ChemBERTa-2, with 15% of tokens in each input randomly masked. We then fine-tune it on Mutag, Mutagen, PTC-FM, PTC-FR, PTC-MM, PTC-MR, and Liver (in Group SELFIES). To evaluate the performance, we compute the average and standard deviation of each metric for each method after 20 rounds of execution. The details of parameter settings is offered in the Supplementary Material D.

B. Results and Analysis

Predictive Performance. Table I presents a comparison of predictive performance across different methods. *MoleX* outperforms all baselines, demonstrating strong robustness and generalizability. By leveraging linear predictor to learn decomposed LLM representations, it achieves 16.9% and 23.1% higher average accuracy compared to LLM and explainable method baselines, respectively. These results highlight the effectiveness of learning with explainable, chemically consistent concepts. Incorporating residual calibration further boosts the average classification accuracy by 11.2% across all datasets. On Mutag, the classification accuracy of the linear predictor improves by 27.8% after integrating LLM-derived representations, followed by an additional 5.5% gain with residual calibration. These results demonstrate that maximizing task-relevant semantics and applying residual calibration enables even simple linear predictor to outperform both GNNs and LLMs. More predictive performance results on six MoleculeNet datasets [74] are provided in the Supplementary Material J.

Explainability Performance. Table II reports the explanation accuracy across different methods. Through learning decomposed LLM representations, *MoleX* significantly outperforms all baselines in explainability. Residual calibration further improves performance, yielding an 8.8% average gain by iteratively correcting mispredicted functional groups and reinforcing chemically accurate ones. On Mutag, the explanation accuracy of the linear predictor improves by 33.4% with LLM decomposition and residual calibration. While other methods perform well on simpler datasets like Mutag but fail on more complex ones, *MoleX* achieves 13.2% higher classification and 16.9% higher explanation accuracy on Liver, demonstrating its ability to *capture the complexity of molecular representations* even with a linear mapping. More explainability performance results on six MoleculeNet datasets [74] are provided in the Supplementary Material J.

Figure 3 visualizes the explanation for a molecule from the Mutag. Domain experts attribute its mutagenicity to an aromatic ring (e.g., benzene) bonded to a functional group such as nitro or carbonyl. *MoleX* accurately reveals this chemically consistent substructure by learning a linear mapping over decomposed LLM representations that encode high-level chemical concepts. Unlike baseline methods that highlight isolated atoms or bonds without structural coherence—for example, PGExplainer marks scattered atoms across multiple benzene rings—*MoleX* yields explanations that are chemically meaningful and structurally complete. More importantly, the uncalibrated linear predictor includes extraneous atoms, while residual calibration corrects these mispredictions and aligns the output with ground truth. This suggests the critical role of calibration in refining explanations and enhancing the explainability of LLM-derived features. Contribution scores further indicate functional group interactions, with the benzene–nitro substructure (i.e., consistent with the ground truth) receiving the highest score, showing its importance in mutagenicity. More visualizations are offered in the Supplementary Material G.

Computational Efficiency. Figure 4 compares execution time across methods. Unlike approaches requiring iterative

TABLE I: Classification accuracy over seven datasets (%). The best and second-best results are shown in bold and underlined, respectively.

Methods	Mutag	Mutagen	PTC-FM	PTC-FR	PTC-MM	PTC-MR	Liver
MolCLR [57]	85.7± 0.4	79.2± 0.6	59.7± 0.5	62.8± 0.5	62.4± 0.4	57.6± 0.5	45.2± 0.9
CGIB [58]	87.1± 0.2	81.5± 0.3	62.3± 0.5	65.7± 0.5	65.1± 0.5	61.1± 0.7	46.9± 0.7
MoSE [59]	88.9± 0.4	<u>83.3± 0.2</u>	<u>63.3± 0.7</u>	68.0± 0.4	67.1± 0.2	62.3± 0.6	<u>50.1± 0.6</u>
FragNet [60]	88.5± 0.5	82.5± 0.4	60.9± 0.8	65.7± 0.8	<u>70.3± 0.3</u>	<u>65.0± 0.2</u>	<u>49.6± 0.6</u>
MomentGNN [61]	89.7± 0.4	81.5± 0.3	59.5± 0.9	68.8± 0.7	65.4± 0.4	60.7± 0.3	47.9± 0.9
S-CGIB [62]	92.0± 0.3	81.3± 0.5	60.8± 0.7	65.1± 0.6	66.3± 0.8	64.5± 0.9	48.3± 1.0
GraphMVP [63]	86.8± 0.2	80.4± 0.4	58.6± 0.4	64.2± 0.3	63.7± 0.5	62.0± 0.4	46.9± 0.4
LLAMA3.1-8b [64]	67.6± 3.4	50.7± 3.6	49.6± 2.6	46.2± 3.8	42.0± 2.8	47.5± 2.8	42.2± 2.2
GPT-4o [65]	73.5± 3.6	51.2± 0.5	52.7± 2.3	53.8± 2.9	48.8± 2.4	53.7± 1.8	44.5± 2.5
ChemBERTa-2 [9]	87.3± 2.7	77.6± 2.2	59.2± 1.9	64.8± 2.2	59.7± 2.8	59.8± 2.4	46.3± 2.3
Logistic Regression	58.3± 1.2	55.4± 0.8	48.4± 1.1	48.3± 1.0	48.7± 1.1	44.9± 1.0	32.5± 0.5
Decision Tree [66]	60.8± 1.7	58.6± 1.5	43.3± 1.0	46.1± 0.7	47.2± 0.7	43.5± 0.5	36.9± 0.8
Random Forest [67]	64.6± 1.9	60.6± 1.5	46.9± 1.2	51.4± 1.5	51.3± 1.8	46.4± 1.1	34.8± 1.9
XGBoost [68]	66.9± 1.2	67.6± 1.4	51.4± 1.3	53.1± 1.4	55.8± 1.2	49.3± 2.1	38.5± 1.8
w/o Calibration	86.1± 2.2	74.4± 1.0	59.7± 2.1	68.9± 1.9	69.3± 2.7	61.2± 2.4	45.0± 2.0
w/ Calibration (Ours)	<u>91.6± 2.0</u>	83.7± 0.9	64.2± 1.4	74.4± 1.9	76.4± 1.8	68.4± 2.3	54.9± 2.4

TABLE II: Explanation accuracy over seven datasets (%). The best and second-best results are marked in bold and underlined, respectively. As LLMs produce uncalibrated, non-discriminative probabilities unsuitable for AUC-based ranking, we omit their explanation accuracy from this table.

Methods	Mutag	Mutagen	PTC-FM	PTC-FR	PTC-MM	PTC-MR	Liver
MolCLR [57]	85.1± 0.2	76.7± 0.3	64.3± 0.6	63.7± 0.3	64.1± 0.2	65.9± 0.8	67.8± 0.3
CGIB [58]	86.1± 0.3	73.6± 0.1	62.3± 0.8	66.0± 0.6	<u>69.0± 0.6</u>	62.0± 0.4	69.1± 0.6
MoSE [59]	79.5± 0.5	81.5± 0.5	<u>69.0± 0.3</u>	66.2± 0.8	<u>68.2± 0.5</u>	59.3± 0.5	68.9± 0.8
FragNet [60]	83.2± 0.4	80.7± 0.4	65.1± 0.2	69.9± 0.4	65.7± 0.4	61.1± 0.7	62.4± 0.4
MomentGNN [61]	81.0± 0.3	78.2± 0.3	67.5± 0.2	62.5± 0.6	63.1± 0.2	<u>70.7± 0.5</u>	70.7± 0.5
S-CGIB [62]	86.7± 0.4	77.3± 0.1	62.4± 0.9	64.9± 0.9	65.5± 0.8	57.5± 0.3	64.2± 0.9
GraphMVP [63]	82.4± 0.2	<u>82.2± 0.6</u>	61.6± 0.4	<u>71.0± 0.3</u>	63.4± 0.5	68.3± 0.3	66.3± 0.3
Logistic Regression	59.2± 0.4	50.6± 0.9	54.4± 0.3	47.7± 0.8	49.9± 0.7	44.3± 0.7	53.8± 0.7
Decision Tree [66]	61.2± 0.2	55.7± 1.0	56.7± 0.8	46.4± 1.1	48.1± 0.9	39.9± 0.8	56.4± 1.0
Random Forest [67]	66.7± 1.2	57.2± 1.2	59.9± 1.7	50.9± 1.2	55.0± 0.8	46.6± 1.1	60.7± 1.4
XGBoost [68]	65.2± 1.2	61.3± 1.1	58.5± 1.8	49.4± 1.8	51.6± 1.3	50.2± 0.8	69.0± 1.4
w/o Calibration	90.0± 0.9	77.7± 1.0	68.0± 1.7	66.6± 1.1	62.0± 1.5	67.5± 1.5	<u>72.0± 2.0</u>
w/ Calibration (Ours)	<u>92.6± 1.7</u>	89.0± 1.2	77.9± 1.5	79.3± 1.4	72.3± 1.7	73.4± 1.3	80.3± 1.4

TABLE III: Classification and explanation accuracy (%) without PCA over seven datasets.

Dataset	Classification Accuracy	Explanation Accuracy
Mutag	94.9 ± 1.6	96.1 ± 3.0
Mutagen	86.4 ± 1.4	91.2 ± 1.6
PTC-FR	78.7 ± 1.2	82.7 ± 1.7
PTC-FM	68.1 ± 1.5	81.1 ± 2.0
PTC-MR	70.5 ± 1.7	76.5 ± 2.6
PTC-MM	80.9 ± 2.7	75.3 ± 2.2
Liver	57.3 ± 1.6	83.8 ± 1.9

network optimization, *MoleX* achieves significantly faster inference via a linear predictor over LLM-derived chemical features. It is at least 10× faster than GNNs and over 300× faster than LLM, while delivering superior performance. Across all datasets, *MoleX* consistently achieves the lowest inference time, demonstrating feasibility for large-scale molecular analysis. By eliminating iterative parameter updates and avoiding the memory overhead of gradient-based optimization, it also substantially reduces GPU usage. This indicates that a linear

mapping over structurally decomposed LLM representations improves efficiency in molecular representation learning.

C. Ablation Studies

How to choose the optimal number of principal components? To obtain compact yet informative representations, we apply PCA to reduce the dimensionality of LLM-derived features. As shown in Figure 5a, both predictive and explanation accuracy improve with more components but begin to plateau beyond 20, suggesting that additional components contribute minimally to model performance. This observation implies that the dominant molecular semantics are captured within the top 20 principal components, while further dimensions primarily encode noise or low-variance information. Including more components increases model complexity and hampers explainability without significant performance gain. Therefore, we retain the top 20 principal components to capture the most significant variance in molecular properties while maintaining a balance between accuracy and explainability.

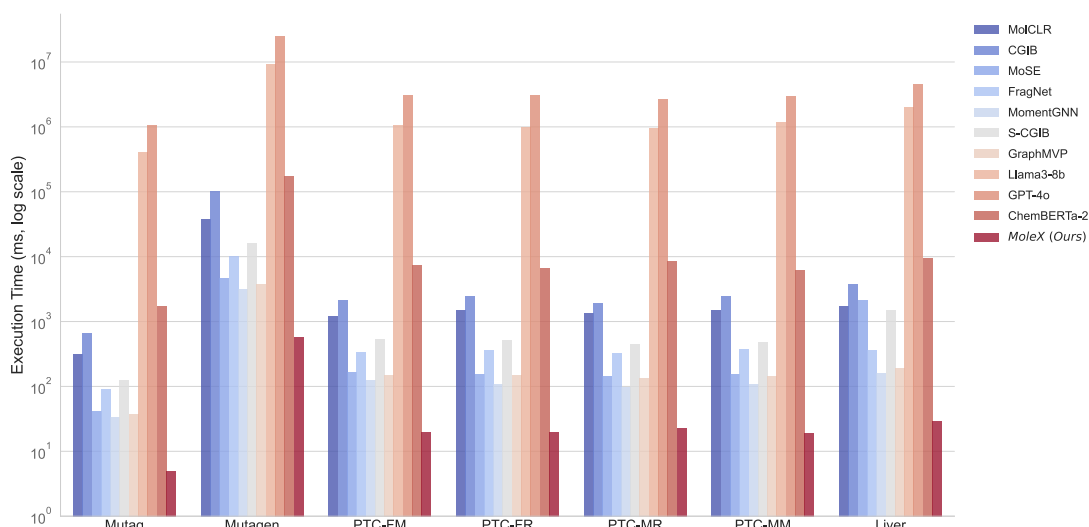
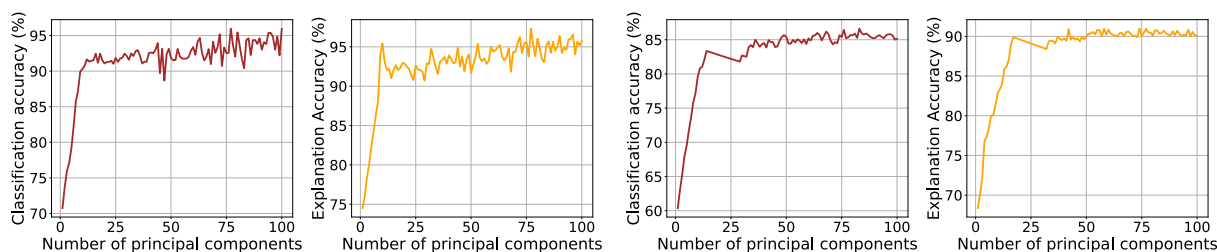


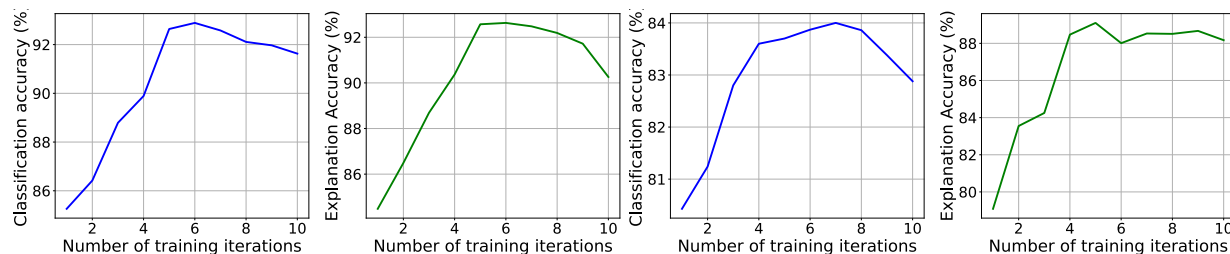
Fig. 4: Execution time comparison on seven datasets. *MoleX* achieves the best efficiency.



(a) Mutag

(b) Mutagen

(a) Effect of the number of principal components on model performance.



(a) Mutag

(b) Mutagen

(b) Effect of the number of residual calibration training iterations on model performance.

How does dimensionality reduction contribute to results?

We show that PCA effectively preserves the most significant dimensions in LLM-derived molecular features. For comparison, we also report model performance across seven datasets *without* dimensionality reduction. As shown in Table III, using only the top 20 principal components yields performance within 5% of that achieved using all 384 components. This result suggests that PCA effectively identifies and retains the most task-relevant semantic directions, while filtering out low-variance or noisy components that contribute little to prediction. By projecting high-dimensional representations onto a compact and explainable subspace, PCA not only preserves predictive power but also enhances model transparency and robustness. The near-equivalent performance under substantial dimensionality reduction highlights the redundancy of many raw LLM representation and supports the hypothesis that molecular properties

are largely governed by a lower-dimensional semantic linear structure. In light of this, PCA serves as an effective mechanism for improving explainability without sacrificing accuracy.

Does the Residual Calibrator Improves Model Performance by training with more iterations? We adopt the training objective defined in Equation (1) to learn a residual calibrator that incrementally corrects the prediction errors made by the base linear predictor. To understand how the number of training iterations affects the effectiveness of the calibrator, we conduct an empirical analysis across four datasets: Mutag, Mutagen, PTC-MR, and Liver. As shown in Figure 5b, model performance consistently improves with additional training iterations, indicating that repeated optimization over our designed loss effectively enhances predictive accuracy. Nevertheless, beyond a certain threshold, the model begins to overfit the training residuals, leading to a decline in

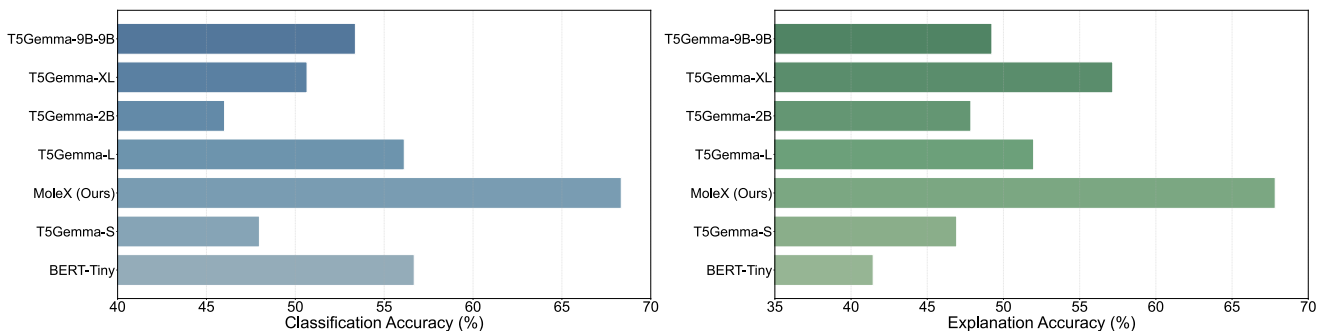


Fig. 6: Effect of LLM model size on downstream performance.

TABLE IV: Classification accuracy across different machine learning models over seven datasets (%).

Method	Mutag	Mutagen	PTC-FR	PTC-FM	PTC-MR	PTC-MM	Liver
Ridge Regression	90.7±1.2	84.1±1.3	72.4±2.0	65.2±2.0	69.8±1.4	77.5±1.5	58.1±1.6
LASSO	91.9±1.7	84.4±0.7	75.1±2.1	65.8±1.7	65.2±0.9	74.2±1.2	58.7±1.8
Linear Discriminant Analysis	89.9±1.9	83.6±1.2	75.2±1.9	65.7±1.9	69.3±1.8	76.8±2.0	57.7±1.3
Support Vector Machine	93.9±1.6	86.6±1.5	73.4±1.9	69.3±2.6	69.5±2.0	78.6±1.3	61.5±2.9
Decision Tree	89.7±2.1	79.5±1.2	72.4±1.8	64.3±2.1	68.5±1.5	74.4±1.4	59.5±2.2
Random Forest	92.8±2.7	84.4±1.7	77.3±2.1	68.6±2.5	71.0±2.2	77.2±2.1	62.7±2.7
Gradient Boosting Machine	94.8±2.1	85.3±1.9	78.9±1.9	69.4±2.8	72.2±2.1	79.2±1.9	63.9±2.6
XGBoost	94.6±2.3	85.0±2.0	78.7±2.2	70.1±2.3	73.4±2.9	78.1±2.1	63.0±2.3
<i>MoleX (Ours)</i>	91.6±2.0	83.7±0.9	74.4±1.9	64.2±1.4	68.4±2.3	76.4±1.8	54.9±2.4

TABLE V: Explanation accuracy across different machine learning models over seven datasets (%).

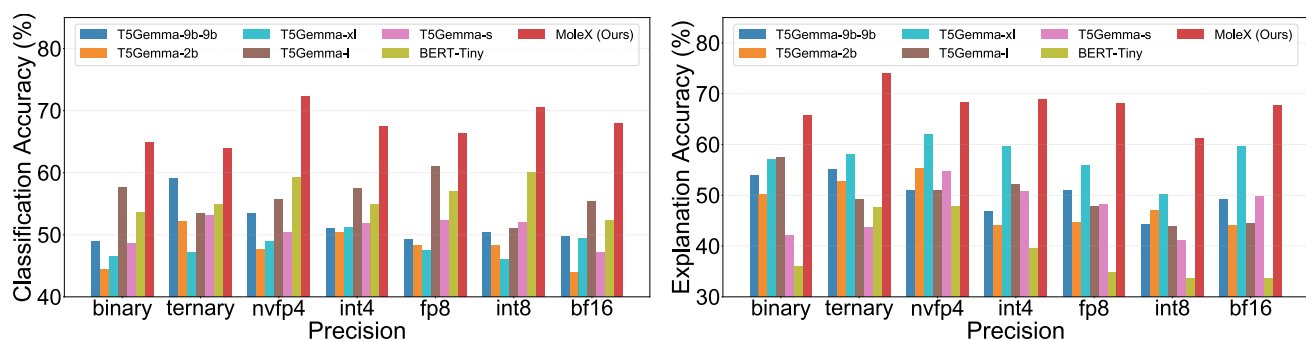
Method	Mutag	Mutagen	PTC-FR	PTC-FM	PTC-MR	PTC-MM	Liver
Ridge Regression	92.8±1.1	89.5±1.3	79.0±1.2	78.1±1.6	72.5±2.5	69.7±2.3	82.4±1.7
LASSO	92.3±1.5	89.6±0.9	76.9±1.8	81.2±1.9	70.4±2.3	70.7±2.1	81.3±1.8
Linear Discriminant Analysis	92.9±1.8	88.5±1.9	80.7±2.3	80.1±2.2	71.7±2.8	71.3±1.6	87.8±1.6
Support Vector Machine	92.0±1.7	92.0±1.6	84.7±2.2	86.3±2.0	80.1±2.3	76.0±2.3	81.9±2.1
Decision Tree	87.6±1.9	89.1±1.5	78.6±2.0	80.7±1.6	73.1±2.1	74.2±1.8	76.0±1.8
Random Forest	93.2±1.9	90.5±1.8	82.1±2.1	84.2±2.2	74.2±2.0	74.5±2.1	81.2±2.0
Gradient Boosting Machine	92.7±2.2	92.4±1.5	82.9±2.3	85.2±2.4	73.9±2.9	77.7±2.6	84.5±2.4
XGBoost	95.6±1.8	90.7±1.7	84.0±2.2	82.0±2.3	74.4±2.7	77.4±2.2	86.2±2.5
<i>MoleX (Ours)</i>	92.6±1.7	89.0±0.9	79.3±2.6	77.9±2.6	73.4±2.8	72.3±3.0	80.3±2.5

generalization performance. This observation suggests a trade-off between correction capacity and overfitting risk. Empirically, we find that 5 training iterations achieve the best performance across datasets. This aligns with our theoretical analysis (detailed in the Supplementary Material E), which shows that repeated residual updates improve the approximation quality up to a point, beyond which the residual function begins to model noise rather than systematic errors. Thus, careful selection of residual calibration training iterations is crucial to realize its benefits without compromising explainability or generalization.

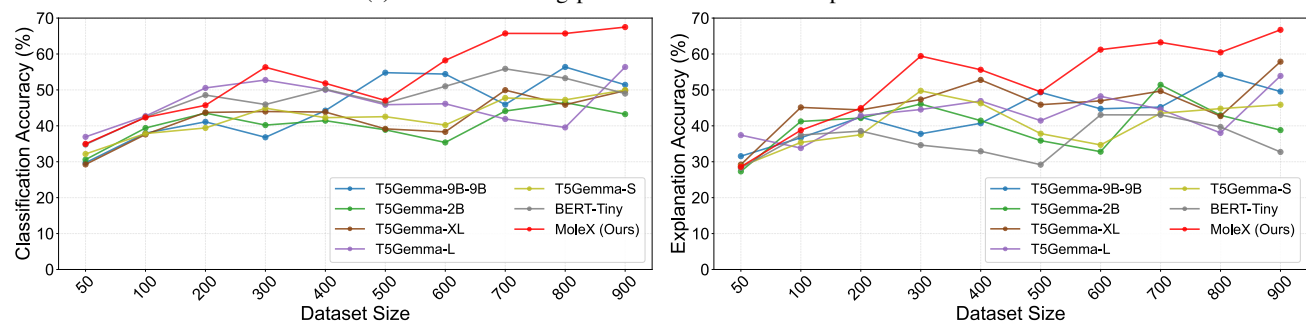
Can alternative model architectures learn the LLM representation? To assess the versatility of LLM-derived molecular representations, we evaluate a broad spectrum of machine learning predictors across seven datasets, using both classification and explanation accuracy as evaluation metrics (Table IV and Table V). Among shallow linear predictors, ridge regression, LASSO, and LDA perform on par with *MoleX*, indicating that LLM representations linearly encode salient chemical features for property prediction. Simple linear predictors thus suffice to extract task-relevant signals. With more expressive predictors: decision trees, random forests, and

gradient boosting (*e.g.*, XGBoost), we observe consistent gains across all datasets. These models capture more complex interactions among LLM features, indicating that the representations encode rich chemical semantics beyond what linear predictors can exploit. This supports the view that LLMs implicitly learn transferable domain knowledge that downstream models of varying complexity can harness.

However, this increased predictive power comes with a trade-off: reduced model explainability. While ensemble models achieve the highest classification accuracy, their black-box nature limits their usefulness in scenarios where explainability is essential, such as scientific discovery or regulatory decision-making. In contrast, linear predictors provide more faithful explanations, particularly when paired with feature attribution (*e.g.*, we can thus clearly attribute molecular properties to specific functional groups). Linearity within LLM latent representations supports clear attribution and downstream performance. It offers a favorable balance between accuracy and explainability, taking advantage of the LLM’s explanatory power without added architectural complexity. Therefore, this permits a principled attribution of how well the LLM encodes



(a) Effect of training precision on downstream performance.



(b) Effect of dataset size on downstream performance.

molecular semantics for chemically grounded modeling.

Under identical conditions, more complex predictors (*e.g.*, more complicated network architectures or modeling assumptions) may deliver higher predictive accuracy, but at the cost of explainability [77], [78]. We thus seek a balance: linearity is a minimal modeling assumption, and when it achieves strong performance, Occam’s razor favors it over added complexity that yields only marginal gains [79], [80]. This is our motivation to probe whether LLM molecular representations exhibit linear relationships, enabling accurate prediction without sacrificing chemically consistent explanations. The gains in explainability and transparent feature attribution afforded by representational linearity outweigh the small incremental improvements delivered by complex predictors that only modestly surpass linear baselines. Decomposing LLM representations via a concept-aligned linear projection produces highly explainable yet strongly predictive molecular semantics. Therefore, investigating and characterizing this latent linearity is central to obtaining explainable molecular representation learning.

D. Scaling the Linear Predictor

In this section, we evaluate the linear predictor’s predictive and explanation performance under varying configurations. Specifically, we vary the LLM parameter size, training precision, and dataset size. Motivated by neural scaling laws [81], we examine how scaling training configurations affects the performance of linear predictor on the four PTC family datasets (PTC-FR, PTC-FM, PTC-MR, and PTC-MM) [71].

Do larger models always deliver better performance?

Models in Figure 6 are ordered top to bottom by decreasing parameter size. Larger foundation models generally improve both classification and explanation accuracy, though not monotonically. For example, the 9B model, T5-Gemma-9B,

shows lower classification accuracy than T5-Gemma-L and BERT-Tiny, probably because its capacity is not well aligned to molecular structure given limited chemical training data. Smaller models near the bottom achieve reasonable classification but weaker explanation accuracy, indicating limited concept decomposition and higher representation noise. Overall, capacity provides headroom but does not directly improve performance. Task-adapted training or fine-tuning is therefore crucial to convert that capacity into better model performance. Essentially, the key to a strong linear predictor is augmenting the foundation LLM with downstream task capability (*e.g.*, via fine-tuning or post-training). Merely increasing model size without appropriate data quality, architectural design, or training strategy yields limited gains.

Does higher training precision improve performance?

Figure 7a reports downstream performance under different training precisions for the linear predictor. Empirically, higher precision enhances model performance [81]. In general, the int8 and bf16 deliver the most stable gains, whereas low precisions (*e.g.*, binary, ternary) degrade performance due to quantization noise. Mixed formats such as nvfp4 and int4 perform surprisingly close to fp8, suggesting that moderate quantization preserves the dominant information in molecular representations that is crucial for property prediction. *MoleX* is the most robust across precisions, remaining reliable even after quantization. Overall, precision has an irregular impact on downstream performance, with some run-to-run variability. Additionally, we observe that larger models are more robust to decreasing precision, whereas smaller models are affected more significantly by precision changes.

Does more training data improve performance?

Figure 7b shows downstream performance for varying training data sizes. In general, adding more training data improves the downstream performance for all models. Increasing the data from 50 to

roughly 300–500 yields the largest gains for both metrics, marking a clear data-scarce to data-sufficient transition. Beyond 500 samples, classification continues to improve but at a slower and model-specific pace, whereas explanation shows sharper gains. Among them, *MoleX* scales best with data, suggesting that its representations convert added data into more linearly decodable information tied to the molecular property prediction. Overall, more data primarily boosts explanation faithfulness and narrows gaps across models, while classification gains are steadier and show diminishing returns beyond a threshold.

VI. CONCLUSION AND DISCUSSION

This work investigates and leverages latent linearity in LLM-derived hidden representations to advance molecular property prediction. In particular, we introduce a chemically consistent decomposition that projects molecular embeddings into a concept space spanned by functional-group vectors, revealing and exploiting hidden linearity in LLMs’ representational geometry. We also propose a residual calibration strategy that captures complex interactions missed by the linear predictor, yielding more accurate predictions and more faithful explanations. Empirically, *MoleX* delivers improved accuracy, explainability, and computational efficiency across multiple benchmark datasets. These results highlight *MoleX* as an effective approach to explainable molecular representation learning and point to a broader path for aligning foundation models with domain science.

However, trade-off between model complexity and performance is still underexplored in molecular representation learning. In this paper, we use a linear predictor, which may underfit complex molecular patterns in some cases. Preliminary comparisons of *MoleX* with more sophisticated models show only marginal gains for the latter. Future work can examine this complexity–performance trade-off in LLM-based molecular representation learning to identify optimal balances between model complexity and downstream performance.

REFERENCES

- [1] J. Xia, L. Zhang, X. Zhu, Y. Liu, Z. Gao, B. Hu, C. Tan, J. Zheng, S. Li, and S. Z. Li, “Understanding the limitations of deep models for molecular property prediction: Insights and solutions,” *Advances in Neural Information Processing Systems*, vol. 36, 2024.
- [2] K. Yang, K. Swanson, W. Jin, C. Coley, P. Eiden, H. Gao, A. Guzman-Perez, T. Hopper, B. Kelley, M. Mathea *et al.*, “Analyzing learned molecular representations for property prediction,” *Journal of chemical information and modeling*, vol. 59, no. 8, pp. 3370–3388, 2019.
- [3] H. Yang, Q. Yao, and J. Kwok, “Curriculum-aware training for discriminating molecular property prediction models,” in *The Thirteenth International Conference on Learning Representations*, 2025.
- [4] G. Zhou, S. Janarthanan, Y. Lu, and P. Hu, “CL-MFAP: A contrastive learning-based multimodal foundation model for molecular property prediction and antibiotic screening,” in *The Thirteenth International Conference on Learning Representations*, 2025.
- [5] Z. Zhong and D. Mottin, “Automatic auxiliary task selection and adaptive weighting boost molecular property prediction,” in *The Thirty-ninth Annual Conference on Neural Information Processing Systems*, 2025.
- [6] yeyunchen and J. Shi, “MIPT: Multilevel informed prompt tuning for robust molecular property prediction,” in *Forty-second International Conference on Machine Learning*, 2025.
- [7] J. Rao, D. Xu, W. Wei, Y. Chen, M. Yang, and Y. Yang, “Quadruple attention in many-body systems for accurate molecular property predictions,” in *Forty-second International Conference on Machine Learning*, 2025.
- [8] S. Chithrananda, G. Grand, and B. Ramsundar, “Chemberta: Large-scale self-supervised pretraining for molecular property prediction,” *arXiv preprint arXiv:2010.09885*, 2020.
- [9] W. Ahmad, E. Simon, S. Chithrananda, G. Grand, and B. Ramsundar, “Chemberta-2: Towards chemical foundation models,” *arXiv preprint arXiv:2209.01712*, 2022.
- [10] S. Li, Z. Liu, Y. Luo, X. Wang, X. He, K. Kawaguchi, T.-S. Chua, and Q. Tian, “Towards 3d molecule-text interpretation in language models,” in *The Twelfth International Conference on Learning Representations*, 2024.
- [11] W. Feng, L. Wang, Z. Lin, Y. Zhu, H. Wang, J. Dong, R. Bai, H. Wang, J. Zhou, W. Peng *et al.*, “Generation of 3d molecules in pockets via a language model,” *Nature Machine Intelligence*, vol. 6, no. 1, pp. 62–73, 2024.
- [12] X. Li, L. Wang, Y. Luo, C. Edwards, S. Gui, Y. Lin, H. Ji, and S. Ji, “Geometry informed tokenization of molecules for language model generation,” in *Forty-second International Conference on Machine Learning*, 2025.
- [13] G. Liu, M. Sun, W. Matusik, M. Jiang, and J. Chen, “Multimodal large language models for inverse molecular design with retrosynthetic planning,” in *The Thirteenth International Conference on Learning Representations*, 2025.
- [14] Y. Zheng, H. Y. Koh, J. Ju, A. T. Nguyen, L. T. May, G. I. Webb, and S. Pan, “Large language models for scientific discovery in molecular property prediction,” *Nature Machine Intelligence*, pp. 1–11, 2025.
- [15] Z. Wu, J. Chen, Y. Li, Y. Deng, H. Zhao, C.-Y. Hsieh, and T. Hou, “From black boxes to actionable insights: a perspective on explainable artificial intelligence for scientific discovery,” *Journal of Chemical Information and Modeling*, vol. 63, no. 24, pp. 7617–7627, 2023.
- [16] S. Kang, G. An, and S. Yoo, “A quantitative and qualitative evaluation of llm-based explainable fault localization,” *Proceedings of the ACM on Software Engineering*, vol. 1, no. FSE, pp. 1424–1446, 2024.
- [17] L. Sharkey, B. Chughtai, J. Batson, J. Lindsey, J. Wu, L. Bushnaq, N. Goldowsky-Dill, S. Heimersheim, A. Ortega, J. Bloom *et al.*, “Open problems in mechanistic interpretability,” *arXiv preprint arXiv:2501.16496*, 2025.
- [18] G. P. Wellawatte and P. Schwaller, “Human interpretable structure-property relationships in chemistry using explainable machine learning and large language models,” *Communications Chemistry*, vol. 8, no. 1, p. 11, 2025.
- [19] P. Hase and M. Bansal, “Evaluating explainable ai: Which algorithmic explanations help users predict model behavior?” *arXiv preprint arXiv:2005.01831*, 2020.
- [20] J. Kunz and M. Kuhlmann, “Properties and challenges of llm-generated explanations,” *arXiv preprint arXiv:2402.10532*, 2024.
- [21] S. Balaji, R. Magar, Y. Jadhav, and A. B. Farimani, “Gpt-molberta: Gpt molecular features language model for molecular property prediction,” *arXiv preprint arXiv:2310.03030*, 2023.
- [22] Y. Zheng, H. Y. Koh, M. Yang, L. Li, L. T. May, G. I. Webb, S. Pan, and G. Church, “Large language models in drug discovery and development: From disease mechanisms to clinical trials,” *arXiv preprint arXiv:2409.04481*, 2024.
- [23] B. Bai, J. Liang, G. Zhang, H. Li, K. Bai, and F. Wang, “Why attentions may not be interpretable?” in *Proceedings of the 27th ACM SIGKDD conference on knowledge discovery & data mining*, 2021, pp. 25–34.
- [24] Z. Wang, Z. Lin, W. Lin, M. Yang, M. Zeng, and K. C. Tan, “Explainable Molecular Property Prediction: Aligning Chemical Concepts with Predictions via Language Models,” *arXiv preprint arXiv:2405.16041*, 2024.
- [25] S. Jain and B. C. Wallace, “Attention is not explanation,” in *Proceedings of the 2019 Conference of the North American Chapter of the Association for Computational Linguistics: Human Language Technologies, Volume 1 (Long and Short Papers)*, 2019, pp. 3543–3556.
- [26] Y. Liu, H. Li, Y. Guo, C. Kong, J. Li, and S. Wang, “Rethinking attention-model explainability through faithfulness violation test,” in *International Conference on Machine Learning*. PMLR, 2022, pp. 13 807–13 824.
- [27] X. Ren, W. Wei, L. Xia, L. Su, S. Cheng, J. Wang, D. Yin, and C. Huang, “Representation learning with large language models for recommendation,” in *Proceedings of the ACM Web Conference 2024*, 2024, pp. 3464–3475.
- [28] F. Petroni, T. Rocktäschel, P. Lewis, A. Bakhtin, Y. Wu, A. H. Miller, and S. Riedel, “Language models as knowledge bases?” *arXiv preprint arXiv:1909.01066*, 2019.
- [29] X. He, X. Bresson, T. Laurent, A. Perold, Y. LeCun, and B. Hooi, “Harnessing explanations: LLM-to-LM interpreter for enhanced text-attributed graph representation learning,” in *The Twelfth International Conference on Learning Representations*, 2024.

- [30] X. Fang, L. Liu, J. Lei, D. He, S. Zhang, J. Zhou, F. Wang, H. Wu, and H. Wang, "Geometry-enhanced molecular representation learning for property prediction," *Nature Machine Intelligence*, vol. 4, no. 2, pp. 127–134, 2022.
- [31] K. Park, Y. J. Choe, and V. Veitch, "The linear representation hypothesis and the geometry of large language models," in *Forty-first International Conference on Machine Learning*, 2024.
- [32] A. Modell, P. Rubin-Delanchy, and N. Whiteley, "The origins of representation manifolds in large language models," *arXiv preprint arXiv:2505.18235*, 2025.
- [33] P. Y. Bruice, *Organic chemistry*. Pearson, 2017.
- [34] R. F. W. Bader, P. L. A. Popelier, and T. A. Keith, "Theoretical definition of a functional group and the molecular orbital paradigm," *Angewandte Chemie International Edition in English*, vol. 33, no. 6, pp. 620–631, 1994.
- [35] I. Siddique, "Exploring functional groups and molecular structures: a comprehensive analysis using ftir spectroscopy," *Chemistry Research Journal*, vol. 9, no. 2, pp. 70–76, 2024.
- [36] R. Gani, "Group contribution-based property estimation methods: advances and perspectives," *Current Opinion in Chemical Engineering*, vol. 23, pp. 184–196, 2019.
- [37] J.-A. Yan and M. Chou, "Oxidation functional groups on graphene: Structural and electronic properties," *Physical Review B—Condensed Matter and Materials Physics*, vol. 82, no. 12, p. 125403, 2010.
- [38] A. H. Cheng, A. Cai, S. Miret, G. Malkomes, M. Phielipp, and A. Aspuru-Guzik, "Group selfies: a robust fragment-based molecular string representation," *Digital Discovery*, vol. 2, no. 3, pp. 748–758, 2023.
- [39] W. Lin, H. Lan, and B. Li, "Generative causal explanations for graph neural networks," in *International Conference on Machine Learning*. PMLR, 2021, pp. 6666–6679.
- [40] P. E. Pope, S. Koulouri, M. Rostami, C. E. Martin, and H. Hoffmann, "Explainability methods for graph convolutional neural networks," in *Proceedings of the IEEE/CVF conference on computer vision and pattern recognition*, 2019, pp. 10772–10781.
- [41] J. Ross, B. Belgodere, V. Chenthamarakshan, I. Padhi, Y. Mroueh, and P. Das, "Large-scale chemical language representations capture molecular structure and properties," *Nature Machine Intelligence*, vol. 4, no. 12, pp. 1256–1264, 2022.
- [42] J. Chen, S. Wu, A. Gupta, and R. Ying, "D4explainer: In-distribution explanations of graph neural network via discrete denoising diffusion," *Advances in Neural Information Processing Systems*, vol. 36, 2024.
- [43] M. Sundararajan, A. Taly, and Q. Yan, "Axiomatic attribution for deep networks," in *International conference on machine learning*. PMLR, 2017, pp. 3319–3328.
- [44] P.-J. Kindermans, S. Hooker, J. Adebayo, M. Alber, K. T. Schütt, S. Dähne, D. Erhan, and B. Kim, "The (un) reliability of saliency methods," *Explainable AI: Interpreting, explaining and visualizing deep learning*, pp. 267–280, 2019.
- [45] J. Adebayo, J. Gilmer, M. Muelly, I. Goodfellow, M. Hardt, and B. Kim, "Sanity checks for saliency maps," *Advances in neural information processing systems*, vol. 31, 2018.
- [46] B. Hoover, H. Strobel, and S. Gehrmann, "exbert: A visual analysis tool to explore learned representations in transformer models," in *Proceedings of the 58th Annual Meeting of the Association for Computational Linguistics: System Demonstrations*, 2020, pp. 187–196.
- [47] S. Serrano and N. A. Smith, "Is attention interpretable?" in *Proceedings of the 57th Annual Meeting of the Association for Computational Linguistics*, 2019, pp. 2931–2951.
- [48] M. T. Ribeiro, S. Singh, and C. Guestrin, "'why should i trust you?' explaining the predictions of any classifier," in *Proceedings of the 22nd ACM SIGKDD international conference on knowledge discovery and data mining*, 2016, pp. 1135–1144.
- [49] S. Agarwal, S. Jabbari, C. Agarwal, S. Upadhyay, S. Wu, and H. Lakkaraju, "Towards the unification and robustness of perturbation and gradient based explanations," in *International Conference on Machine Learning*. PMLR, 2021, pp. 110–119.
- [50] F. Sebastiani, "Machine learning in automated text categorization," *ACM computing surveys (CSUR)*, vol. 34, no. 1, pp. 1–47, 2002.
- [51] A. A. Alemi, I. Fischer, J. V. Dillon, and K. Murphy, "Deep variational information bottleneck," in *International Conference on Learning Representations*, 2022.
- [52] D. P. Kingma, T. Salimans, and M. Welling, "Variational dropout and the local reparameterization trick," *Advances in neural information processing systems*, vol. 28, 2015.
- [53] L. McInnes, J. Healy, and J. Melville, "Umap: Uniform manifold approximation and projection for dimension reduction," *arXiv preprint arXiv:1802.03426*, 2018.
- [54] H. Abdi and L. J. Williams, "Principal component analysis," *Wiley interdisciplinary reviews: computational statistics*, vol. 2, no. 4, pp. 433–459, 2010.
- [55] T. Hastie, R. Tibshirani, J. H. Friedman, and J. H. Friedman, *The elements of statistical learning: data mining, inference, and prediction*. Springer, 2009, vol. 2.
- [56] C. R. Rao and H. Toutenburg, "Linear models," in *Linear Models: Least Squares and Alternatives*. Springer, 1995, pp. 3–18.
- [57] Y. Wang, J. Wang, Z. Cao, and A. Barati Farimani, "Molecular contrastive learning of representations via graph neural networks," *Nature Machine Intelligence*, vol. 4, no. 3, pp. 279–287, 2022.
- [58] N. Lee, D. Hyun, G. Na, S. Kim, J. Lee, and C. Park, "Conditional graph information bottleneck for molecular relational learning," *arXiv preprint arXiv:2305.01520*, 2023.
- [59] L. Bao, E. Jin, M. Bronstein, Í. Í. Ceylan, and M. Lanzinger, "Homomorphism counts as structural encodings for graph learning," *International Conference on Learning Representations*, 2025.
- [60] G. Panapitiya, P. Gao, C. M. Maupin, and E. G. Saldanha, "Fragnet: A graph neural network for molecular property prediction with four layers of interpretability," *arXiv preprint arXiv:2410.12156*, 2024.
- [61] C. Kanatsoulis and A. Ribeiro, "Counting graph substructures with graph neural networks," in *The twelfth international conference on learning representations*, 2024.
- [62] V. T. Hoang, O. Lee *et al.*, "Pre-training graph neural networks on molecules by using subgraph-conditioned graph information bottleneck," *arXiv preprint arXiv:2412.15589*, 2024.
- [63] S. Liu, H. Wang, W. Liu, J. Lasenby, H. Guo, and J. Tang, "Pre-training molecular graph representation with 3d geometry," in *ICLR 2022 Workshop on Geometrical and Topological Representation Learning*, 2022.
- [64] A. Dubey, A. Jauhri, A. Pandey, A. Kadian, A. Al-Dahle, A. Letman, A. Mathur, A. Schelten, A. Yang, A. Fan *et al.*, "The llama 3 herd of models," *arXiv preprint arXiv:2407.21783*, 2024.
- [65] J. Achiam, S. Adler, S. Agarwal, L. Ahmad, I. Akkaya, F. L. Aleman, D. Almeida, J. Altenschmidt, S. Altman, S. Anadkat *et al.*, "Gpt-4 technical report," *arXiv preprint arXiv:2303.08774*, 2023.
- [66] J. R. Quinlan, "Induction of decision trees," *Machine learning*, vol. 1, pp. 81–106, 1986.
- [67] L. Breiman, "Random forests," *Machine learning*, vol. 45, pp. 5–32, 2001.
- [68] T. Chen and C. Guestrin, "Xgboost: A scalable tree boosting system," in *Proceedings of the 22nd acm sigkdd international conference on knowledge discovery and data mining*, 2016, pp. 785–794.
- [69] A. K. Debnath, R. L. Lopez de Compadre, G. Debnath, A. J. Shusterman, and C. Hansch, "Structure-activity relationship of mutagenic aromatic and heteroaromatic nitro compounds. correlation with molecular orbital energies and hydrophobicity," *Journal of medicinal chemistry*, vol. 34, no. 2, pp. 786–797, 1991.
- [70] C. Morris, N. M. Kriege, F. Bause, K. Kersting, P. Mutzel, and M. Neumann, "Tudataset: A collection of benchmark datasets for learning with graphs," *arXiv preprint arXiv:2007.08663*, 2020.
- [71] H. Toivonen, A. Srinivasan, R. D. King, S. Kramer, and C. Helma, "Statistical evaluation of the predictive toxicology challenge 2000–2001," *Bioinformatics*, vol. 19, no. 10, pp. 1183–1193, 2003.
- [72] R. Liu, X. Yu, and A. Wallqvist, "Data-driven identification of structural alerts for mitigating the risk of drug-induced human liver injuries," *Journal of cheminformatics*, vol. 7, pp. 1–8, 2015.
- [73] W. Lin, H. Lan, H. Wang, and B. Li, "Orphicx: A causality-inspired latent variable model for interpreting graph neural networks," in *Proceedings of the IEEE/CVF Conference on Computer Vision and Pattern Recognition*, 2022, pp. 13 729–13 738.
- [74] Z. Wu, B. Ramsundar, E. N. Feinberg, J. Gomes, C. Geniesse, A. S. Pappu, K. Leswing, and V. Pande, "Moleculenet: a benchmark for molecular machine learning," *Chemical science*, vol. 9, no. 2, pp. 513–530, 2018.
- [75] Z. Ying, D. Bourgeois, J. You, M. Zitnik, and J. Leskovec, "Gnnexplainer: Generating explanations for graph neural networks," *Advances in neural information processing systems*, vol. 32, 2019.
- [76] J. J. Irwin, T. Sterling, M. M. Mysinger, E. S. Bolstad, and R. G. Coleman, "Zinc: a free tool to discover chemistry for biology," *Journal of chemical information and modeling*, vol. 52, no. 7, pp. 1757–1768, 2012.
- [77] M. A. Poole and P. N. O'Farrell, "The assumptions of the linear regression model," *Transactions of the Institute of British Geographers*, pp. 145–158, 1971.

- [78] A. F. Schmidt and C. Finan, “Linear regression and the normality assumption,” *Journal of clinical epidemiology*, vol. 98, pp. 146–151, 2018.
- [79] K. P. Murphy, *Machine learning: a probabilistic perspective*. MIT press, 2012.
- [80] T. Hastie, R. Tibshirani, and M. Wainwright, “Statistical learning with sparsity,” *Monographs on statistics and applied probability*, vol. 143, no. 143, p. 8, 2015.
- [81] J. Kaplan, S. McCandlish, T. Henighan, T. B. Brown, B. Chess, R. Child, S. Gray, A. Radford, J. Wu, and D. Amodei, “Scaling laws for neural language models,” *arXiv preprint arXiv:2001.08361*, 2020.